Healing pattern
After vertical ramus osteotomy
By time intervals
On micro-computed tomography

Oh, Min Seok

The Graduate School

Yonsei University

Department of Dental Science

Healing pattern

After vertical ramus osteotomy

By time intervals

On micro-computed tomography

Directed by Professor Jung, Young-Soo

A Doctoral Dissertation

Submitted to the Department of Dental Science

and the Graduate School of Yonsei University

in partial fulfillment of the

requirements for the degree of

Doctor of Philosophy in Dental Science

Oh, Min Seok

December 2014

This certifies that the dissertation

of Oh, Min Seok is approved.

Thesis Supervisor: Jung, Young-Soo

Baik, Hyoung-Seon

Kim, Kee-Deog

Jung, Han Sung

Nam, Woong

Department of Dental Science

The Graduate School, Yonsei University

December 2014

감사의 글

먼저 저를 항상 인도해 주신 하나님께 감사를 드립니다.

그 누구보다도, 부족한 제가 논문을 완성할 수 있도록 아낌없는 배려와 세심한 지도로 이끌어 주신 정영수 지도 교수님께 진심으로 감사 드립니다. 또한 논문이 완성될 때까지 지속적인 관심과 도움을 주셨던 백형선 교수님, 김기덕 교수님, 정한성 교수님, 남웅 교수님께도 깊은 감사의 말씀을 드립니다. 그리고 한 사람의 구강악안면외과 의사로서 거듭날 수 있도록 기회를 주시고 인도해 주신 故 이의웅 교수님, 이충국 교수님, 박형식 교수님, 차인호 교수님, 이상휘 교수님, 김형준 교수님께도 깊은 감사 드립니다.

실험에 큰 도움을 주고 논문 전반에 걸쳐서 조언을 아끼지 않은 정휘동 교수님, 그리고 학업을 무사히 마치도록 배려해주시고 격려해 주신 김기정 원장님께도 깊은 감사를 드립니다. 박사 논문을 쓰는 동안 도움을 주신 제노스의 장정선 팀장님,박원서 교수님, 김동욱 선생, 그리고 의국 후배 선생님들께도 감사를 드립니다. 항상 옆에서 걱정해주던 위즈 치과 직원 여러분에게도 이 자리를 빌어 감사의 마음을 전합니다.

항상 사랑과 믿음으로 지켜봐 주시고 기도로 응원해 주시는 부모님과 형, 누나, 언제나 걱정해 주시는 장모님께도 깊은 감사의 마음을 전합니다. 마지막으로 늘 곁에서 힘이 되어주고, 살아가는 이유가 되는 사랑하는 아내 슬기와 큰 딸 지민, 둘째 유민, 막내 하민이에게 고마움을 전하며 이 기쁨을 나누고 싶습니다.

2015년 2월
오민석

TABLE OF CONTENTS

LIST OF FIGURES

LIST OF TABLES

ABSTRACT

Healing pattern after vertical ramus osteotomy by time intervals on micro-computed tomography

Oh, Min Seok

Department of Dental Science
The Graduate School, Yonsei University

(Directed by Professor Jung, Young-Soo, DDS, PhD)

Vertical ramus osteotomy (VRO) in mandible is a preferred method for mandibular prognathic patients. Few experimental studies of osseous healing and remodeling of VRO, unlike proper healing of fracture, have been conducted under similar clinical situations. Many clinicians using this procedure are thus greatly dependent on their own experiences. To better understand the healing pattern on adult beagle dogs after vertical ramus osteotomy, they were euthanized and observed at 1st week, 2nd week, 3rd week, 4th week, 6th week, and 8th week respectively. Each specimen was scanned in a micro-computed tomography – an imaging tool regarded as the gold standard for evaluation of bone morphology and microarchitecture and several parameters were calculated. We then reached the following conclusions:

1. The amount of newly formed bone increased up to 4^{th} week, decreased slowly up to 6^{th} week, and decreased sharply after 6^{th} week.
2. The new bone volume around the distal segment was larger than that around the proximal segment up to 6^{th} week and vice versa at 8^{th} week.
3. The parameters in the new bone around the distal segment up to 6^{th} week, such as BV (bone volume), BV/TV (bone volume fraction), BS/BV (specific bone surface), Tb.N (trabecular number), Tb.Sp (trabecular separation) as well as the parameters in the new bone around the proximal segment, such as Tb.Th (trabecular thickness) were statistically significant in demonstrating increased strength with the maturation of new bone.

Together with the above results, the healing pattern after vertical ramus osteotomy showed active generation of new bone up to 4^{th} week, followed by remodeling. New bone volume around the distal segment was larger than that around the proximal segment up to 6^{th} week and vice versa at 8^{th} week. Clinically, preservation of the distal segment vasculature which contribute to the early healing of VRO, importantly should be taken into consideration.

Key words: VRO, micro-computed tomography, healing pattern

Healing pattern after vertical ramus osteotomy by time intervals on micro-computed tomography

Oh, Min Seok

Department of Dental Science
The Graduate School, Yonsei University

(Directed by Professor Jung, Young-Soo, DDS, PhD)

I. INTRODUCTION

Vertical ramus osteotomy (VRO) in mandible is a preferred method for mandibular prognathic patients. (Ghali and Sikes, 2000) It is performed from sigmoid notch to mandibular angle vertically, avoiding mandibular foramen. The distal segment is then driven backward followed by the lateral overlapping of proximal segment with temporomandibular joint . (Fonseca RJ, 2009)

It has generally been considered essential for proper healing of fracture that displaced fragments be fixed into each cortical to cortical, marrow to marrow surface and that the formation of primary callus be encouraged in a stationary state. Unlike the general fracture healing process, VRO induces a cortex-to-cortex healing process. VRO was initially performed with wire fixation of bony fragments. (Alling, 1965) With developments in internal rigid fixation, however, VRO came to be used with screws and plates. (Kraut, 1988; Paulus and Steinhauser, 1982) Nevertheless, non-fixation method are preferred, for bony fragments in the pterygomasseteric sling, which, unlike long bone, heal well without fixation. Such methods also avoid complications in rigid fixation, such as temporomandibular disorders (TMDs) due to inproper position of the proximal segment. Bell reported that except in case of excessive mandibular setback, additional internal rigid fixation was largely unnecessary. (Bell.W.H, 1992)

The objection has been raised that in non-fixation methods such as in the case of non - fixation of fragments after VRO, there is no bony union but rather a movable state or fibrous union. (Huebsch and Wellington, 1967) However, there have to date been few reports of non-union or fibrous-union cases. Moreover the healing process between the proximal and distal segment is not the same as in other bony healing processes given the the cortex-to-cortex healing and complete dissection of the periosteums. (Reitzik, 1983) Boyne (1966) reported that excellent callus formation and bony union were obtained by VRO with bony fixation. Bell and Kennedy (1976) reported that continuous circulation to proximal segment is necessary to retain osseous viability, their experiments supporting the clinical practice of pedicling condylar segment to the articular capsule and lateral pterygoid muscle. In those experiments the overlapping of both fragments driving the proximal segment anteriorly was not the same as the clinical method of driving the distal segment backward. Lee and Park (1997) reported an experiment under almost identical clinical condtions using histologic observations and magnetic resonance imaging (MRI).

There have been no further reports of VRO healing patterns since Arimoto et al. (2013), which used conventional computed tomography. Few experimental studies of osseous healing and remodeling of VRO have been conducted under similar clinical situations. Many clinicians using this procedure are thus greatly dependent on their own experiences.

Among recent imaging tools, micro-computed tomography (micro-CT) has become the “gold standard” for evaluation of bone morphology and microarchitecture in mice and other small models. (Bouxsein et al., 2010) Micro-CT uses X-ray attenuation data acquired at multiple viewing angles reconstruct three dimensional (3D) representation of the specimen that characterizes the spatial distribution of material density. There are several advantages to using micro-CT to assess bone mass and morphology, as listed below.

1. Micro-CT scanner achieve an isotropic voxel size of as low as a few micrometers, sufficient for investigating structures such as bone trabeculae with widths of approximately 30 to 50 ㎛. (Martín Badosa et al., 2003)
2. Micro-CT allows direct 3D measurement of trabecular morphology, such as thickness and separation, rather than inferring these values based on 2D stereologic models, as is done with standard histologic evaluations. (Hildebrand and Ruegsegger, 1997; Laib et al., 1997)
3. Compared with 2D histology, a significantly larger volume of interest can be analyzed.

4. Measurement can be performed much faster than with typical histologic analyses using undecalcified bone specimens.
5. As assessment of bone morphology by micro-CT scanning is noninvasive, specimen can be used for subsequently assays, such as histology or mechanical testing.
6. Micro-CT scans allow estimates of bone tissue mineralization by comparing X-ray attenuation in bone with that of hydroxyapatite standards. This voxel-based mineral density data can be used to create micro-finite element models to estimate mechanical behavior.

In this experiment, micro-CT was used to observe the osseous healing pattern, confirm previous experiments by measuring several parameters, and obtain new findings. This experimental study investigates the chronology of the bone healing process after VRO with early mobilization in adult beagle dogs in a clinical situation using micro-CT.

II. MATERIALS AND METHODS

All experiments were performed under protocols approved by the Institutional Animal Care and Use Committee at the Yonsei University Medical Center (2012-0064).

1. Animal care

Seven 8-month-old male beagle dogs, weighing between 11.9 and 13.5 kg (average 12.57±0.57 kg) were used. In general, beagle dogs over 6 months have reached sexual maturation and are regarded as adult dogs. These were provided regular fodder before surgery, intravenous fluid (5% D/W 1 l/day) 1week after surgery due to immobilization of mandible, and soft diet plus liquid food after that.

2. Anesthesia

Seven animals were operated under intravenous injection of 2ml zoletil and xylazine at a 6:4 ratio as induction drugs and under isoflurane – induced endotracheal ansesthesia.

3. Vertical ramus osteotomy

The surgical area was shaved and draped in standard surgical fashion, cleaned with 10% povidone-iodine solution, and quartered with sterile towels. The mandible ramus was exposed via extraoral approach. Masseter muscle and periosteum was reflected laterally and the mandible was exposed buccally. Vertical ramus osteotomy was made from sigmoid notch to the 2~3cm anterior of angle of mandible using a Stryker reciprocating saw and copious saline irrigation. Special attention was paid to avoiding injury of the inferior alveolar neurovascular bundle. The proximal segment was then made to overlap the lateral aspect of the distal segment, which was driven backward. (Fig. 1) These procedures were performed on the ramus of mandible without interfragmental fixations. The wound was closed in layers with absorbable sutures in the deep layers and nylon skin sutures.

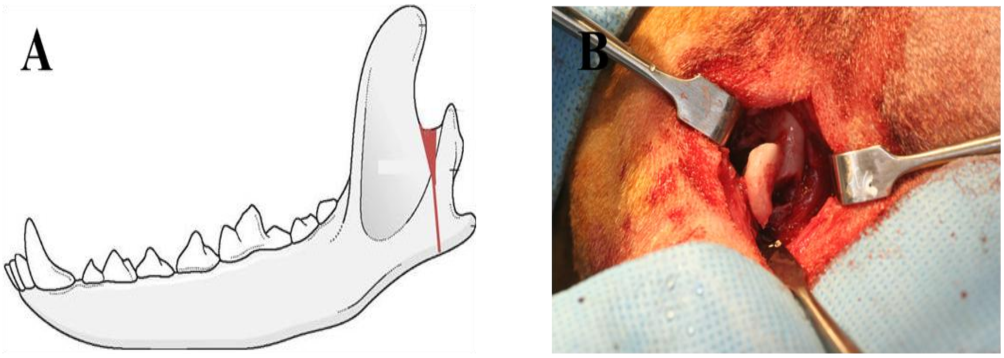

Figure 1. Vertical ramus osteotomy design (A) and overlapping segments (B)

4. Postoperative care & preparation of specimens

To prevent postoperative infection, the dogs received antibiotics (enrofloxacine 0.2ml/kg, Komipharm international Co., Ltd., Korea) administered intramuscularly for 3 days, tight elastic bandages being applied to the head of the experimental animals for 1 week postoperatively to immobilize their mandibles during callus formation. At 8^{th} postoperative day, bi-maxillary fixations by elastic bandage were cleared. The dogs were euthanized with suxamethonium chloride hydrate 50mg/ 1ml (Komipharm international Co., Ltd., Korea) intravenous injection at postoperative 1^{st} week, 2^{nd} week, 3^{rd} week, 4^{th} week, 6^{th} week and 8^{th} week respectively, and the experimental specimens were carefully harvested en bloc including their adjacent soft tissue. (Fig. 2) There were 7 experimental animals in total, consisting of 6 animals in addition to 1 animal killed at postoperative 2^{nd} week due to unfavorable bony contact.

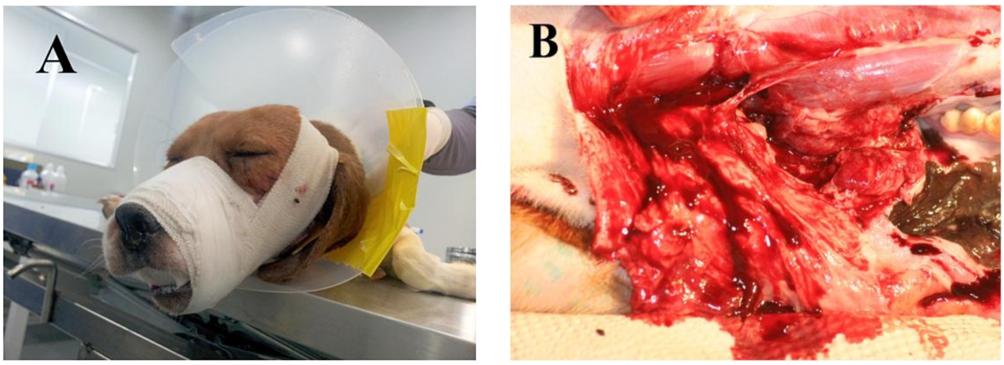

Figure 2. Immobilization of mandible (A) and harvesting of specimen (B)

5. Micro-computed tomography scanning and analysis

In order to place the specimens consistently inside the holder, they were fixed with elastic tape. The micro-CT scanner SkyScan1173 (Bruker-CT, Kartuizerwsweg 3B 2550 Kontich, Belgium) acquired tomographic images under air media for 30 minutes at energy settings of 130 kV and 30 μA, integration time of 250 ms, filtration by 1.0mm aluminium, beam hardening correction 40%, and 40 μm pixel size. The cross-section reconstruction was made using Nrecon® software (ver. 1.6.6.0). For each micro-CT scan, a data set of average 166 cross –section grey level (intensity values 0 and 255) images was produced, with a slice separation of one pixel (40 μm). (Fig. 3)

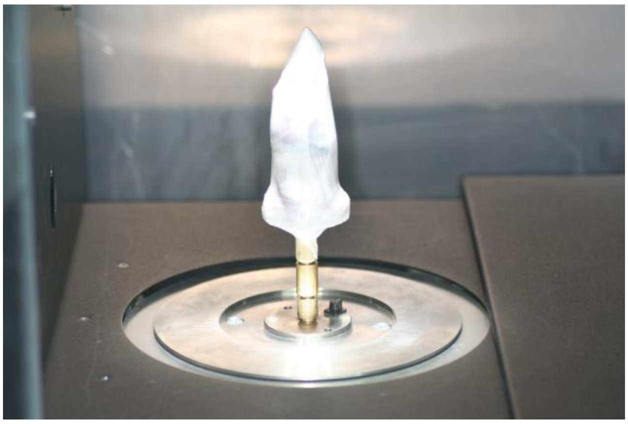

Figure 3. Fixing specimen by elastic tape into micro-CT scanner holder

Comparing original 2D images with the segmented micro-CT scan images, a proper threshold was selected (82~255 mg HA/cm^3). Once the distal segment was separated from the proximal segment, the regions of interest including each newly formed bone were selected and measured with CT Analyzer (ver. 1.14.41) software. 3D images were reconstructed with CT Vol (ver.2.2.3.0) software. (Fig. 4)

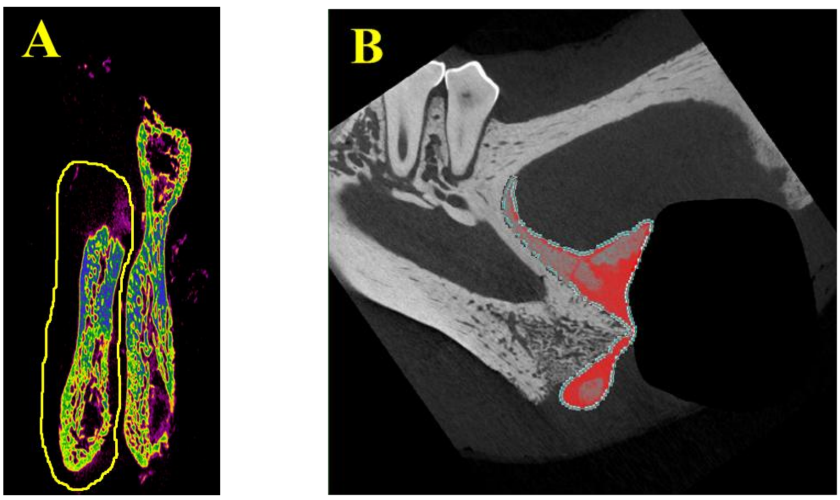

Fig 4. Separating proximal segment part from distal segment (A) and Selecting each region of interest (B)

The 3D bone morphology parameters are defined as:

TV (total volume): volume of the entire region of interest

BV (bone volume): volume of the region segmented as bone

BS (bone surface): surface of the region segmented as bone

BV/TV (bone volume fraction): ratio of the segmented bone volume to the total volume of the region of interest

BS/BV (specific bone surface): ratio of the segmented bone surface to the segmented bone volume

BS/TV (bone surface density): ratio of the segmented bone volume to the total volume of the region of interest

SMI (structure model index): an indicator of the structure of trabecule. SMI will be 0 for parallel plates and 3 for cylindrical rods

Tb.N (trabecular number): measure of the average number of trabecule per unit length using direct 3D methods

Tb.Th (trabecular thickness): mean thickness of trabecule assessed using direct 3D methods

Tb.Sp (trabecular separation) : mean distance between trabecule assessed using direct 3D methods

6. Statistical Analysis

SPSS software for Windows, version 18.0 (SPSS, Chicago, USA), was used for all statistical analyses. Kendall’s tau correlation coefficient analysis and Spearman’s rank correlation coefficient analysis were used to obtain the correlation between each parameter and time (week). Each analysis should be operated in case of the small number of experimental specimens. Kendall’s tau correlation analysis is known to be more reliable than Spearman’s rank correlation coefficient analysis.

III. RESULTS

1. Overview of serial bone healing in 3D reconstruction images

At 1st week, no callus between segments was observed. Partial bony union in some parts was observed from 2nd week, the surface texture of 3D reconstruction images having changed according to the apposition of callus on the buccal side of the distal fragment. From 3rd week, the fracture line began to disappear in patches and soft callus appeared. There was a tendency for the fracture line to disappear and gap at 4th week. At 6th week bony calluses between the proximal and distal segments were mineralized, and at 8th week, with the resorption of most of the newly generated callus, the bony callus between segments was remodeled into cortical bone. (Fig. 5 and 6)

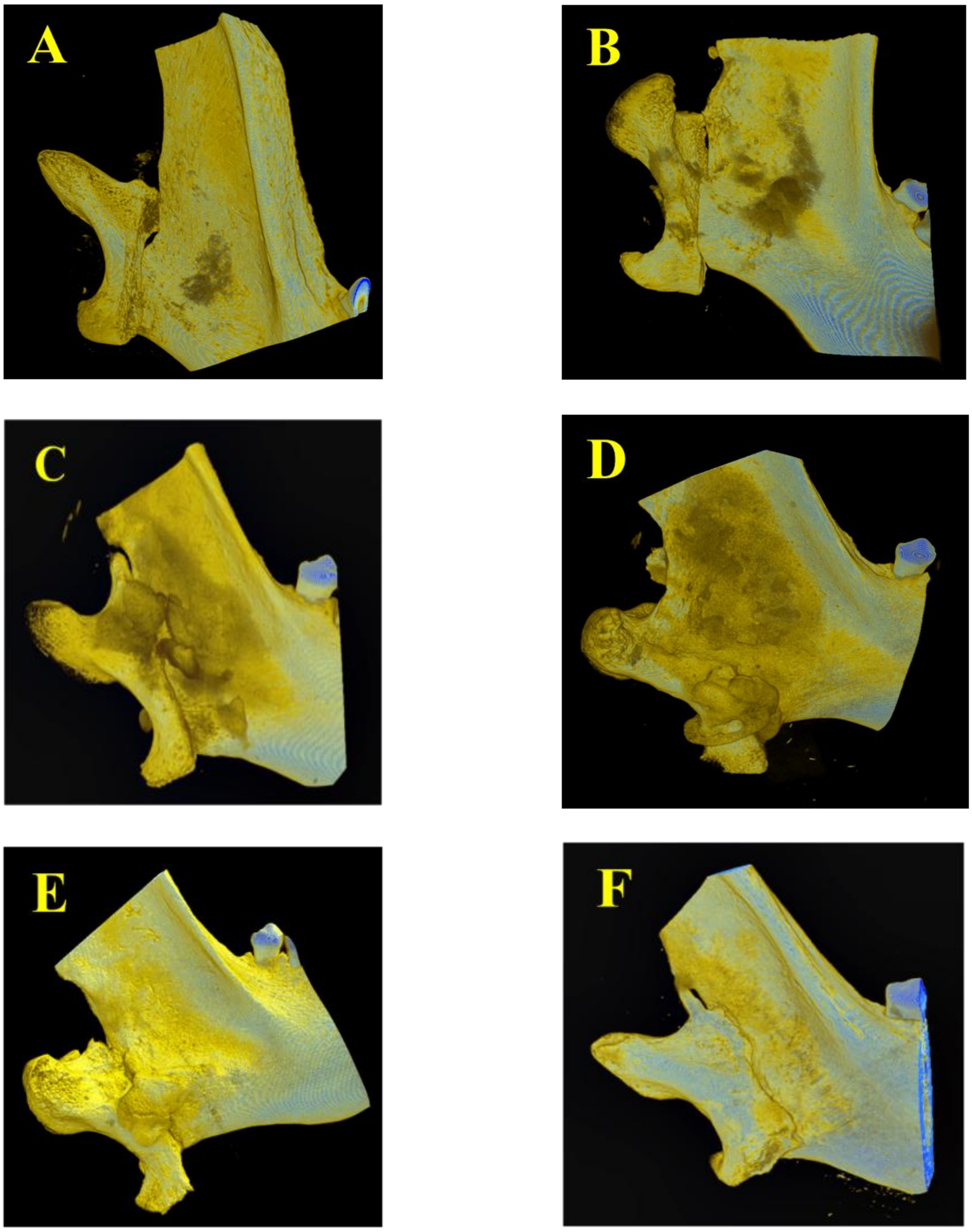

Fig 5. 3D reconstruction images at 1st (A), 2nd (B), 3rd (C), 4th (D), 6th (E) and 8th weeks(F) from buccal aspect

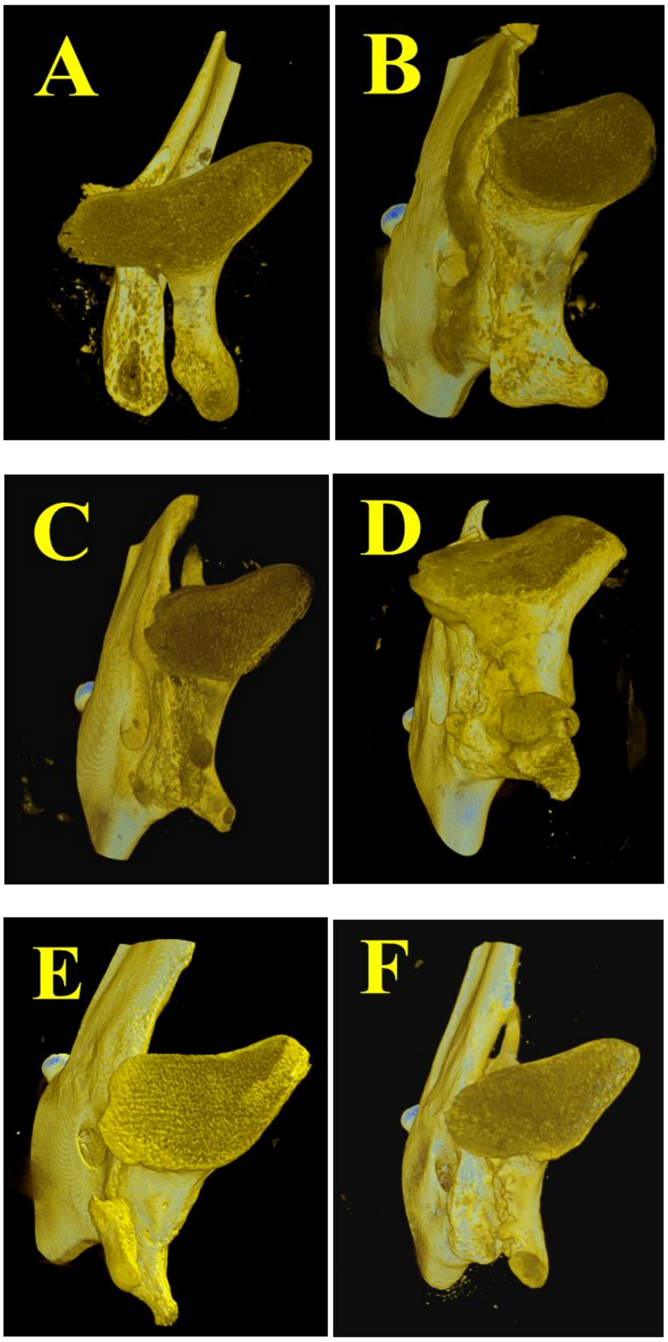

Fig 6. 3D reconstruction images at 1st (A), 2nd (B), 3rd (C), 4th (D), 6th (E), and 8th weeks (F) from condylar aspect

Color coding based on X-ray intensity in the 3D reconstruction images reveals the bony change. For example, the enamel with high X-ray intensity appears white whereas air, with no intensity, appear black. Figure 7, the blue in the middle of each fragment was regarded as cortical bone surface and the red in the gap between segments as newly formed bone. Red appear in the gap between fragments and elsewhere in figure 6 (A) (1st week), while the red has diminished and the bony bridge area shows more green than red in X-ray intensity. These phenomena indicate that the new bone has been transformed into mature bone. (Fig.7)

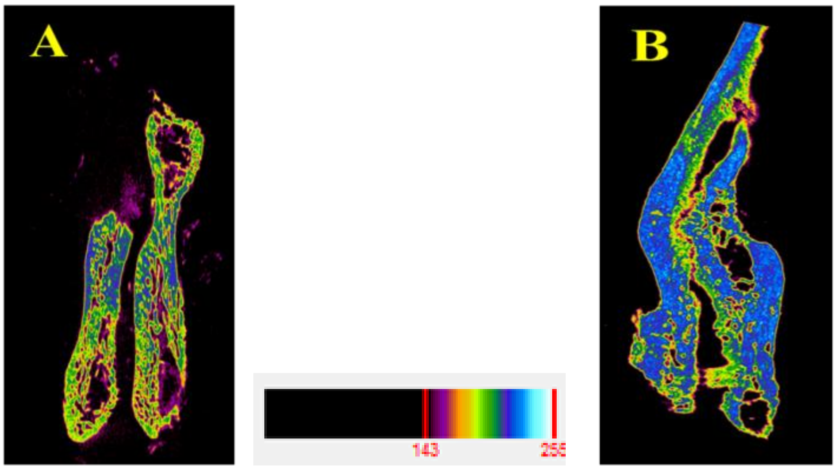

Figure 7. Healing pattern comparison between 1st week (A) and 8th week (B). This color-coding images were converted by original 3D reconstruction images according to x-ray intensity. X-ray intensity became higher toward white color.

2. New bone volume

The amount of newly formed bone increased up to 4 weeks and decreased sharply after 6 weeks. Once the distal segment was separated from the proximal segment and the newly formed bone measured in both segments, new bone volume around the distal segment was larger than that around the proximal segment up to 6th week and vice versa at 8th week. (Fig.8) The total new bone volume and the new bone volume around the distal segment had a significant correlation with time in Spearman's rank correlation coefficient analysis ($p < 0.05$) and no significant correlation with time in Kendall's tau correlation coefficient analysis. The new bone volume around the proximal segment had no significant correlation with time. The result at 8th week was excluded due to excessive variation.

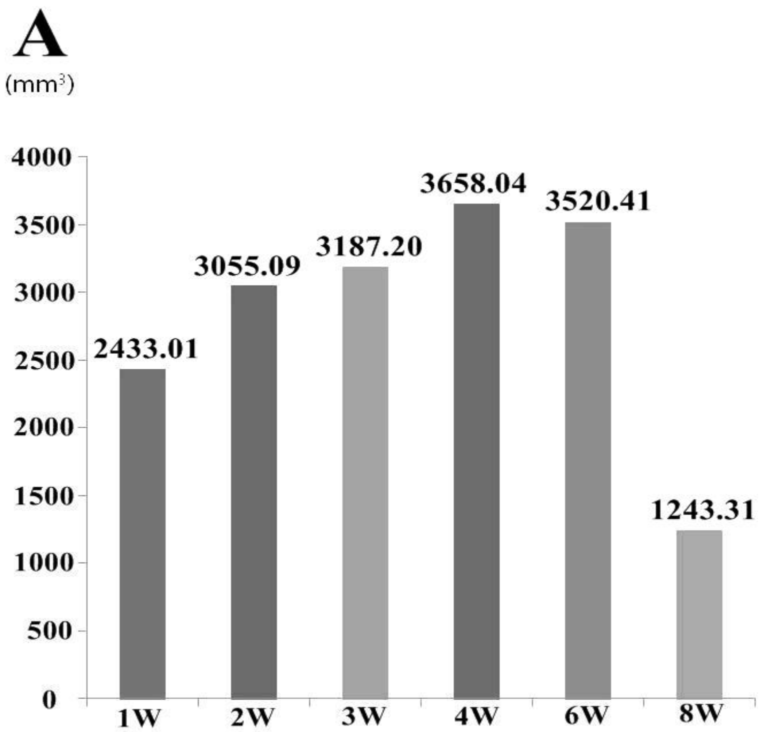

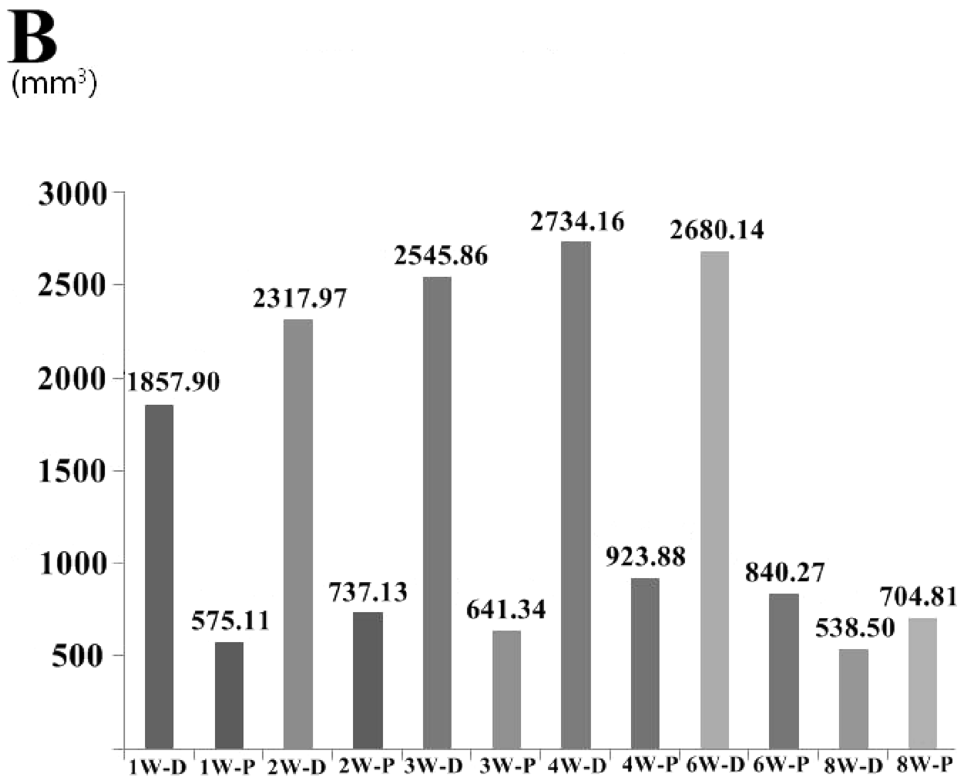

Fig 8. Chronological total (A) and new bone volume change for each part (B). Bone volume increased up to 4th week and decreased sharply after 6th week. The 8th week specimen was excluded due to excessive variation

W, week; D, around the distal segment; P, around the proximal segment

3. The other parameters

Table 1. The parameters for assessing new bone quantity.

	Week	BV/TV(D)	BV/TV(P)	BS/BV(D)	BS/BV(P)	BS/TV(D)	BS/TV(P)
	1	4.53	3.77	2.20	7.55	0.10	0.28
	2	3.51	1.02	2.13	5.51	0.07	0.06
	3	7.47	3.88	2.03	5.88	0.15	0.23
	4	8.15	6.28	1.83	3.95	0.15	0.25
	6	8.83	2.70	1.93	4.91	0.17	0.13
	8	1.07	6.55	4.70	4.42	0.05	0.29
Kendall's tau b	**corr.coef. f**	0.8	0.2	-0.8	-0.6	0.738	-0.2
	p	0.05	0.624	0.05	0.142	0.077	0.624
Spearman's rho	**corr.coef. f**	0.9	0.2	-0.9	-0.8	0.872	-0.3
	p	$\mathbf{0.037}^{**}$	0.747	$\mathbf{0.037}^{*}$	0.104	0.054	0.624

*, $P < 0.05$; **, $P < 0.01$; Kendall's tau-b corr. coef., Kendall's tau-b correlation coefficient ; Spearman's rho corr. coef., Spearman's rank correlation coefficient; BV, bone volume (mm^3); TV, total volume (mm^3); BS, bone surface (mm^2); BV/TV, bone volume fraction (%); BS/BV, specific bone surface (1/mm); BS/TV, bone surface density (1/mm); D, around distal segment; P, around proximal segment; 8th week specimen results were excluded due to excessive variation

BV/TV and BS/BV in the new bone around the distal segment had a significant correlation with time in Spearman's rank correlation coefficient analysis ($p < 0.05$) and no significant correlation with time in Kendall's tau correlation coefficient analysis. BS/TV in the new bone around the distal segment and BV/TV, BS/BV, BS/TV in new bone around the proximal segment had no significant correlation with time. The results at 8th week were excluded due to excessive variation.

Table 2. The parameters for assessing new bone quality around the distal segments

	Week	SMI(D)	Tb.N(D)	Tb.Th(D)	Tb.Sp(D)	DA(D)
	1	-1.19	0.03	1.37	12.90	3.19(0.68)
	2	0.91	0.02	1.91	16.57	1.95(0.48)
	3	-3.81	0.05	1.62	10.92	3.45(0.71)
	4	-2.44	0.05	1.76	10.70	4.09(0.75)
	6	0.93	0.05	1.89	9.73	3.25(0.69)
	8	3.19	0.01	1.29	13.32	5.78(0.82)
Kendall's tau b	**Corr.coef. f.**	0.2	0.8	0.4	- 0.8	0.4
	p	0.624	0.05	0.327	0.05	0.327
Spearman's rho	**Corr.coef. f.**	0.2	0.9	0.4	- 0.9	0.6
	p	0.747	**0.037***	0.505	**0.037***	0.285

*, P < 0.05; **, P < 0.01; Kendall's tau-b corr. coef., Kendall's tau-b correlation coefficient ; Spearman's rho corr. coef., Spearman's rank correlation coefficient; BV, bone volume (mm^3); TV, total volume (mm^3); BS, bone surface (mm^2); BV/TV, bone volume fraction (%); BS/BV, specific bone surface (1/mm); BS/TV, bone surface density (1/mm); D, around distal segment; P, around proximal segment; 8^{th} week specimen results were excluded due to excessive variation

Tb.N in new bone around the distal segment had a significant correlation with time in Spearman's rank correlation coefficient analysis ($p < 0.05$) and no significant correlation with time in Kendall's tau correlation coefficient analysis. Tb.Sp had a significant negative correlation with time in Spearman's correlation coefficient analysis. SMI, Tb.Th, and DA in the new bone around the distal segment had no significant correlation with time. 8^{th} week results were excluded due to excessive variation.

Table 3. The parameters for assessing new bone quality around the proximal segments

	Week	SMI(P)	Tb.N(P)	Tb.Th(P)	Tb.Sp(P)	DA(P)
	1	0.55	0.05	0.71	8.87	1.34(0.25)
	2	-0.82	0.01	0.80	23.48	1.12(0.11)
	3	0.90	0.05	0.81	9.71	1.42(0.29)
	4	-1.55	0.06	1.03	8.97	1.38(0.27)
	6	0.26	0.02	1.10	14.26	1.62(0.38)
	8	-0.19	0.07	1.00	8.99	1.67(0.40)
Kendall's tau b	**Corr.coef. f.**	-0.2	0	1	0.2	0.6
	p	0.624	1	**< 0.05***	0.624	0.142
Spearman's rho	**Corr.coef. f.**	-0.3	0	1	0.3	0.8
	p	0.624	1	**< 0.01***	0.624	0.104

*, P < 0.05; **, P < 0.01; Kendall's tau-b corr. coef., Kendall's tau-b correlation coefficient ; Spearman's rho corr. coef., Spearman's rank correlation coefficient; BV, bone volume (mm^3); TV, total volume (mm^3); BS, bone surface (mm^2); BV/TV, bone volume fraction (%); BS/BV, specific bone surface (1/mm); BS/TV, bone surface density (1/mm); D, around distal segment; P, around proximal segment; 8^{th} week specimen results were excluded due to excessive variation

Tb.Th in the new bone around the proximal segment had a significant correlation with time in both Kendall's tau correlation coefficient analysis (p < 0.05) and Spearman's rank correlation coefficient analysis(p < 0.01) and SMI, Tb.N, Tb.Sp, DA in the new bone around the proximal segment had no significant correlation with time. 8^{th} week results were excluded due to excessive variation.

III. DISCUSSION

Until recently most bone healing studies were done with histologic methods which had been the standard for experiments of involving trabecular and cortical bone architecture. Many previous experimental studies, particularly Lee and Park (1997) assessed the healing of VRO with histologic methods. Although histologic analyses have provided unique insights into cellularity and dynamic indices of bone remodeling, they were limited with respect to quantitative assessment of bone microarchitecture and direct 3D measurement of trabecular morphology.

The standard method for quantitatively describing bone architecture is the calculation of morphometric indices, also referred to as “quantitative morphometry.” In the past, the microarchitectural characteristics of trabecular and cortical bone were investigated by examining 2D sections of bone biopsies and calculating morphometric parameters using sterologic methods. (Parfitt, 1983) Whereas some measurements such as BV/TV and BS/TV can be obtained directly from 2D images, several parameters, including trabecular thickness (Tb.Th), trabecular separation (Tb.Sp), and trabecular number (Tb.N) are derived indirectly after assuming a fixed-structure model such as a rod-like or plate-like structure. These highly idealized models can be considered two ends of a spectrum, the real architecture being a mixture of both rods and plates, precise composition depending on skeletal site, disease state, treatment, and age. Thus correlations among Tb.Th, Tb.Sp, and Tb.N measurements made using 2D methods require assumptions about the underlying structure and 3D model-independent measurements of these parameters are only modest and vary with skeletal sites. Deviations in trabecular structure from the assumed plate or rod models will therefore lead to unpredictable errors in indirectly derived parameters. (Hildebrand and Ruegsegger, 1997; Laib et al., 1997)

In this regard, directly measuring 3D structure with micro-CT has an advantage in terms of volumetric measurement. Also, several studies have established the excellent reproducibility and accuracy of micro-CT measurement of bone morphology, the accuracy having been evaluated by comparison with traditional 2D histomorphometry measures in both animal (Alexander et al., 2001; Barbier et al., 1999; Bonnet et al., 2009; Kapadia et al., 1998; Waarsing et al., 2004) and human specimens. (Akhter et al., 2007; Chappard et al., 2005; Fanuscu and Chang, 2004; Kuhn et al., 1990; Muller et al., 1998) These studies show that 2D and 3D morphologic measurements by micro-CT are generally highly correlated with those from 2D histomorphometry. For instance, Muller et al. (1998) reported very high correlations (r = 0.84~0.92) and low percentage differences between the two methods for measurements of human iliac biopsies. However, some studies report that micro-CT measurements overestimate trabecular thickness relative to histomorphometric measurements. This may be attributed to several factors including inadequate resolution of micro-CT images relative to trabecular size, the use of a plate model to estimate trabecular thickness in 2D histomorphometry versus direct 3D methods in micro-CT, poor threshold selection, and the fact that 3D micro-CT measurements of trabecular intersections, tend to increase trabecular thickness values compared with measurements made only on trabecular struts. (Chappard et al., 2005) Nonetheless, the high correlation between the two techniques provide a strong rationale for the use of micro-CT to assess skeletal morphometry.

The basic parameter in this experiment, the amount of newly formed bone increased up to 4 weeks and decreased sharply by 6 weeks. Lee and Park (1997) reported that up to the 4th week the calluses around the fragments, especially inferiorly and posteriorly had grown and united, and that at 8th week new bone had decreased dramatically with general bony resorption by many osteoclasts. This study shows that the decrease accelerates from 6th week to 8th week relative to 4th week to 6th week.

The unique aspect of our experimental design is the separation of the distal from the proximal segment in the investigation of new bone formation. Because the bony union was incomplete, the new bone formation area could be divided into two regions. It was found that the new bone volume around the distal segment exceeded that around the proximal segment up to 6th week and vice versa at 8th week. As noted in Boyne (1966), Bell & Kennedy (1977), and Lee and Park (1997), the generated calluses after VRO approximate subperiosteal callus, increasing owing to the great proliferation of osteoblasts such as fibroblasts. In other words, the newly formed subperiosteal callus may result from remaining periosteum. (Daum et al., 1985; Reitzik, 1983; Simmons, 1985) The transformation of the fibroblast in the adjacent connective tissue occurs by osteoinduction. (Alberius and Johnell, 1991; Urist, 1965) The greater amount of new bone around the distal segment compared to that around the proximal segment in this experiment may be due to the minimal reflection of the distal segment compared with the proximal segment, abundant periosteum and a relatively rich blood supply to temporal muscle, medial pterygoid muscle, and the inferior alveolar neurovascular bundle.

This would also explain the smaller resorption in the new bone of the proximal segment compared to that in the distal segment: whereas most new bone posterior and lateral to its fragment consisting of most part of distal segment had been resorbed by osteoclast, in the proximal segment most new bone, consisting of uniting callus, changed into hard callus rather than being resorbed. Thus the resorption of the proximal segment, which had a relatively small volume of new bone in the posterior and lateral surface was smaller than that of distal segment. (Lee and Park, 1997) Moreover, the phenomena of bony necrosis in the cortical bone and the ischemic necrosis of bone marrow also have contributed to the difference in resorption. Bell et al. observed these phenomena in mandible after VRO and other procedures (Bell and Kennedy, 1976; Bell and Levy, 1970; Bell and Schendell, 1977), the phenomena disappearing over 2 months (Foster et al., 1951; Rhinelander, 1968) Cortical bony necrosis is known to result from heat by drilling in osteotomy and delayed revascularization from adjacent soft tissue due to loss of blood supply by the periosteum reflection as well as bone marrow amputation. In particular, a delay in revascularization and primary callus formation in the inferior end of the proximal segment has been observed. (Lee and Park, 1997) These several observations account for the new bone volume around the proximal segment being smaller than that around the distal segment for the first 6 weeks. A delay in revascularization and primary callus formation in the inferior end of the proximal segment occurred. Since after 6^{th} week new bone was replaced by revascularization without severe bony resorption, there was much less bony resorption around the proximal segment than around the distal segment from 6^{th} week to 8^{th} week.

BV/TV (bone volume fraction) is the ratio of segmented bone volume to the total volume of the region of interest. In theory, whereas the trabecular bone could not exceed 100% due to its porous structure, the cortical bone might be nearly 100%. In general, the strength of new bone increases according to the chronology of bony maturation. Further, bone strength is known to be closely related to bone volume. In this experiment, BV/TV had a significant tendency to increase with time up to 6th week. This result is consistent with previous reports that among the parameters related to bone volume, BV/TV had a distinct linear correlation with bone strength. (Huh KH, 2005; Kleerekoper et al., 1985)

Another basic measure is of bone surface (BS), conventionally computed by triangulation of the object surface using a marching-cubes algorithm. Bone surface density (BS/TV) and specific bone surface (BS/BV) can of course be derived by dividing the bone surface by the total volume or bone volume, respectively. BS/BV is a useful parameter for characterizing structural complexity. In case of a rough trabecular structure, perforated trabecular plate, and a low ratio of plate to rod, the BS/BV ratio will be high. In case of high BV/TV and low BS/BV, trabecular bone structure is thick and has a plate-like composition. Conversely, low BV/TV and high BS/BV, indicates trabecular bone with a rough, rod-like structure. (Moon, 2003) In this study, BS/BV in the distal segment decreased with time. The increased BV/TV ratio correlated with a thicker and more plate-like (rather than rod-like) trabecular bone, consistent with the maturation of new bone. (Halloran et al., 2002) The minimal set of variables needed to characterize trabecular regions consists of bone volume fraction (BV/TV), trabecular thickness (Tb.Th), trabecular separation (Tb.Sp), and trabecular number (Tb.N) because these can be found in most publications and are to some extent comparable with classical histomorphometric variables. (Bouxsein et al., 2010) Trabecular separation (Tb.Sp) and trabecular thickness (Tb.Th) measure mean thickness, distance, and density of trabecular regions in each specimen based on 3D calculations using a sphere-fitting method whereby the spheres are fitted to the object for thickness measurement and the spheres are fitted to the background for separation. (Hildebrand and Ruegsegger, 1997) Trabecular number (Tb.N) is computed as the inverse of the mean distance between the mid-axes of the structure, as derived via the distance-transformation method. A low Tb.N indicates a rough trabecular bone structure and is distinctly correlated with BV/TV. Tb.Sp tends to be inversely proportionate to BV/TV and Tb.N. Low Tb.Sp correlates with, trabecular structures in close position, trabecular bone with a compact structure. Conversely, trabecular bone has a rough structure in the case of high Tb.Sp. (Moon, 2003)

In this experiment, based on an analysis of micro-CT parameters, trabecular number (Tb.N)(D) and trabecular thickness (Tb.Th)(P) increased significantly and trabecular separation (Tb.Sp)(D) had decreased significantly up to 6th week. This means that the spacing of trabeculae was reduced (Tb.Sp↓), thickness and number of trabeculae were increasing (Tb.Th, Tb.N↑). This is consistent with new bone becoming mature with time. Tb.Th (D), Tb.N (P), and Tb.Sp(P) yielded no significant results in this experiment. If a greater number of specimens had been investigated, a firm result could have been achieved.To estimate the plate-like versus rod-like characteristics of trabecular bone structure, a structure model index (SMI) was developed which designated perfect plates as 0, perfect rods as 3, perfect spheres as 4, concavity as positive, and convexity as negative. This index is a key indicator of reduction of trabeculae due to osteoporosis, characterized by the transition from plate-like structure to rod-like. Degree of anisotropy (DA) may explain a significant number of mechanical properties of the 3D structure, together with bone volume fraction (BV/TV) (Giesen et al., 2003; Odgaard, 1997; Sugita et al., 1999) Isotropy is a measure of 3D symmetry or the presence or absence of preferential alignment of structures along a particular directional axis. DA is calculated using the mean intercept-length ellipsoid method, that is, the ratio of maximum radius to minimum radius. In general, the closer trabecula comes to isotropy, the more evenly disturbed the pressure on the trabecular bone and thus the more resistance to strength. Further, note that if the trabeculae have more consistent directional structure, that is, has a larger DA, the bone strength decreases. (Huh KH, 2005) In this study, SMI and DA yielded no statistically significant and stable results due to variations in bone formation in different regions, from the uppermost heads of the condyle to the inferior border of mandibular ramus. Also, as the occlusal force of the experimental dogs could have no effect on the healing callus, the DA parameter as influenced by such force was rendered insignificant. (Giesen et al., 2003) It is known from several reports that bone strength has a positive correlation with bone volume, trabecular number, and trabecular thickness. (Giesen et al., 2003; Odgaard, 1997; Sugita et al., 1999) Thus despite not having studied mechanical strength in this experiment, we may assume that the strength of the newly formed bone increase incrementally.

We found that the amount of newly formed bone increased up to 4 weeks and decreased sharply after 6 weeks. Separately measuring the newly formed bone in the distal and proximal segments, the new bone volume around the distal segment was found to exceed that around the proximal segment up to 6th week and vice versa at 8th week. We regretted not finding a general tendency by mean analyses of numerous experimental subjects and not conducting primate tests, which would have greater relevance to clinical application in humans. Hereafter, if it is possible to conduct micro-CT scans of the same specimen in vivo chronologically, we will obtain results without inter-individual errors.

IV. Conclusion

Vertical ramus osteotomy (VRO) in mandible is a preferred method for mandibular prognathic patients. To better understand the healing pattern on adult beagle dogs after vertical ramus osteotomy, they were euthanized and observed at 1^{st} week, 2^{nd} week, 3^{rd} week, 4^{th} week, 6^{th} week, and 8^{th} week respectively. Each specimen was scanned in a micro-computed tomography scanner and several parameters were calculated. We then reached the following conclusions.

1. The amount of newly formed bone increased up to 4^{th} week, decreased slowly up to 6^{th} week, and decreased sharply after 6^{th} week.
2. The new bone volume around the distal segment was larger than that around the proximal segment up to 6^{th} week and vice versa at 8^{th} week.
3. The parameters in the new bone around the distal segment up to 6^{th} week, such as BV (bone volume), BV/TV (bone volume fraction), BS/BV (specific bone surface), Tb.N (trabecular number), Tb.Sp (trabecular separation) as well as the parameters in the new bone around the proximal segment, such as Tb.Th (trabecular thickness) were statistically significant in demonstrating increased strength with the maturation of new bone.

Together with the above results, the healing pattern after vertical ramus osteotomy showed active generation of new bone up to 4^{th} week, followed by remodeling. New bone volume around the distal segment was larger than that around the proximal segment up to 6^{th} week and vice versa at 8^{th} week. Clinically, preservation of the distal segment vasculature which contribute to the early healing of VRO, importantly should be taken into consideration.

V. Reference

Akhter MP, Lappe JM, Davies KM, Recker RR: Transmenopausal changes in the trabecular bone structure. *Bone* 41(1): 111-116, 2007.

Alberius P, Johnell O: Repair of intra-membranous bone fractures and defects in rats. Immunolocalization of bone and cartilage proteins and proteoglycans. *J Craniomaxillofac Surg* 19(1): 15-20, 1991.

Alexander JM, Bab I, Fish S, Muller R, Uchiyama T, Gronowicz G, et al.: Human parathyroid hormone 1-34 reverses bone loss in ovariectomized mice. *J Bone Miner Res* 16(9): 1665-1673, 2001.

Alling CC: Correction of Mandibular Prognathism by Open, Oblique Sliding Osteotomies of the Rami. *J Oral Surg* 23: 199-211, 1965.

Arimoto S, Hasegawa T, Kaneko K, Tateishi C, Furudoi S, Shibuya Y, et al.: Observation of osseous healing after intraoral vertical ramus osteotomy: focus on computed tomography values. *J Oral Maxillofac Surg* 71(9): 1602 e1601-1602 e1610, 2013.

Barbier A, Martel C, de Vernejoul MC, Tirode F, Nys M, Mocaer G, et al.: The visualization and evaluation of bone architecture in the rat using three-dimensional X-ray microcomputed tomography. *J Bone Miner Metab* 17(1): 37-44, 1999.

Bell WH, Kennedy JW, 3rd: Biological basis for vertical ramus osteotomies--a study of bone healing and revascularization in adult rhesus monkeys. *J Oral Surg* 34(3): 215-224, 1976.

Bell WH, Levy BM: Revascularization and bone healing after anterior mandibular osteotomy. *J Oral Surg* 28(3): 196-203, 1970.

Bell WH, Schendel SA: Biologic basis for modification of the sagittal ramus split operation. *J Oral Surg* 35(5): 362-369, 1977.

Bell.W.H: Modern practice in orthognathic and reconstructive surgery. W.B. Saunders, 1992.

Bonnet N, Laroche N, Vico L, Dolleans E, Courteix D, Benhamou CL: Assessment of trabecular bone microarchitecture by two different x-ray microcomputed tomographs: a comparative study of the rat distal tibia using Skyscan and Scanco devices. *Med Phys* 36(4): 1286-1297, 2009.

Bouxsein ML, Boyd SK, Christiansen BA, Guldberg RE, Jepsen KJ, Muller R: Guidelines for assessment of bone microstructure in rodents using micro-computed tomography. *J Bone Miner Res* 25(7): 1468-1486, 2010.

Boyne PJ: Osseous healing after oblique osteotomy of the mandibular ramus. *J Oral Surg* 24(2): 125-133, 1966.

Chappard D, Retailleau-Gaborit N, Legrand E, Basle MF, Audran M: Comparison insight bone measurements by histomorphometry and microCT. *J Bone Miner Res* 20(7): 1177-1184, 2005.

Cline HE, Dumoulin CL, Hart HR, Jr., Lorensen WE, Ludke S: 3D reconstruction of the brain from magnetic resonance images using a connectivity algorithm. *Magn Reson Imaging* 5(5): 345-352, 1987.

Daum WJ, Simmons DJ, Chang SL, Lehman RC, Webster D: Effect of fixation devices on radiostrontium clearance in the intact canine femur. *Clin Orthop Relat Res* (194): 306-312, 1985.

Fanuscu MI, Chang TL: Three-dimensional morphometric analysis of human cadaver bone: microstructural data from maxilla and mandible. *Clin Oral Implants Res* 15(2): 213-218, 2004.

Feldkamp LA, Goldstein SA, Parfitt AM, Jesion G, Kleerekoper M: The direct examination of three-dimensional bone architecture in vitro by computed tomography. *Journal of bone and mineral research* 4(1): 3-11, 1989.

Fonseca RJ TT, Marciani RD.: Oral and maxillofacial surgery. In: Orthognathic surgery, esthetic surgery, cleft and craniofacial surgery. 1st ed. RJ F, ed. Elsevier, St. Louis:. 2009.

Foster LN, Kelly RP, Jr., Watts WM, Jr.: Experimental infarction of bone and bone marrow; sequelae of severance of the nutrient artery and stripping of periosteum. *J Bone Joint Surg Am* 33-A(2): 396-406, 1951.

Ghali GE, Sikes JW, Jr.: Intraoral vertical ramus osteotomy as the preferred treatment for mandibular prognathism. *J Oral Maxillofac Surg* 58(3): 313-315, 2000.

Giesen EB, Ding M, Dalstra M, van Eijden TM: Reduced mechanical load decreases the density, stiffness, and strength of cancellous bone of the mandibular condyle. *Clin Biomech (Bristol, Avon)* 18(4): 358-363, 2003.

Halloran BP, Ferguson VL, Simske SJ, Burghardt A, Venton LL, Majumdar S: Changes in bone structure and mass with advancing age in the male C57BL/6J mouse. *J Bone Miner Res* 17(6): 1044-1050, 2002.

Hildebrand T, Ruegsegger P: Quantification of Bone Microarchitecture with the Structure Model Index. *Comput Methods Biomech Biomed Engin* 1(1): 15-23, 1997.

Huebsch RF, Wellington JS: Osseous healing in dog mandibles with and without decortication. *Oral Surg Oral Med Oral Pathol* 23(2): 236-240, 1967.

Huh KH PM, Yi WJ, Heo MS, Lee SS, Choi SC: Relationship between trabecular strength and three-dimensional architecture in the pig mandible using microcomputed tomography. *Korean J Oral Maxillofac Radiol* 35(3): 167-173, 2005.

Kapadia RD, Stroup GB, Badger AM, Koller B, Levin JM, Coatney RW, et al.: Applications of micro-CT and MR microscopy to study pre-clinical models of osteoporosis and osteoarthritis. *Technol Health Care* 6(5-6): 361-372, 1998.

Kleerekoper M, Villanueva AR, Stanciu J, Rao DS, Parfitt AM: The role of three-dimensional trabecular microstructure in the pathogenesis of vertebral compression fractures. *Calcif Tissue Int* 37(6): 594-597, 1985.

Kraut RA: Stabilization of the intraoral vertical osteotomy using small bone plates. *J Oral Maxillofac Surg* 46(10): 908-910, 1988.

Kuhn JL, Goldstein SA, Feldkamp LA, Goulet RW, Jesion G: Evaluation of a microcomputed tomography system to study trabecular bone structure. *J Orthop Res* 8(6): 833-842, 1990.

Laib A, Hildebrand T, Hauselmann HJ, Ruegsegger P: Ridge number density: a new parameter for in vivo bone structure analysis. *Bone* 21(6): 541-546, 1997.

Lee S-H, Park, Hyung-Sik: Bone healing process in early mobilization after vertical ramus osteotomy of the mandible in adult dogs. *J Korean Assoc Oral Maxillofac Surg* 23(3): 434-457, 1997.

Markel MD, Wikenheiser MA, Morin RL, Lewallen DG, Chao EY: Quantification of bone healing. Comparison of QCT, SPA, MRI, and DEXA in dog osteotomies. *Acta Orthop Scand* 61(6): 487-498, 1990.

Martín Badosa E, Amblard D, Nuzzo S, Elmoutaouakkil A, Vico L, Peyrin F: Excised bone structures in mice: imaging at three-dimensional synchrotron radiation micro CT. *Radiology* 229(3): 921-928, 2003.

Moon H-S, Won Y-E, Kim K-D, Lee S-W, Paik M-H, Kook H-G, Jung M-G: 3D analysis of mandibular trabecular microstructure. *Implantology* (10): 13-24, 2003.

Muller R, Van Campenhout H, Van Damme B, Van Der Perre G, Dequeker J, Hildebrand T, et al.: Morphometric analysis of human bone biopsies: a quantitative structural comparison of histological sections and micro-computed tomography. *Bone* 23(1): 59-66, 1998.

Odgaard A: Three-dimensional methods for quantification of cancellous bone architecture. *Bone* 20(4): 315-328, 1997.

Parfitt AM: Assessment of trabecular bone status. *Henry Ford Hosp Med J* 31(4): 196-198, 1983.

Paulus GW, Steinhauser EW: A comparative study of wire osteosynthesis versus bone screws in the treatment of mandibular prognathism. *Oral Surg Oral Med Oral Pathol* 54(1): 2-6, 1982.

Reitzik M: Cortex-to-cortex healing after mandibular osteotomy. *J Oral Maxillofac Surg* 41(10): 658-663, 1983.

Rhinelander FW: The normal microcirculation of diaphyseal cortex and its response to fracture. *J Bone Joint Surg Am* 50(4): 784-800, 1968.

Simmons DJ: Fracture healing perspectives. *Clin Orthop Relat Res* (200): 100-113, 1985
.

Sugita H, Oka M, Toguchida J, Nakamura T, Ueo T, Hayami T: Anisotropy of osteoporotic cancellous bone. *Bone* 24(5): 513-516, 1999.

Urist MR: Bone: formation by autoinduction. *Science* 150(3698): 893-899, 1965.

Waarsing JH, Day JS, Weinans H: An improved segmentation method for in vivo microCT imaging. *J Bone Miner Res* 19(10): 1640-1650, 2004.

ABSTRACT (IN KOREAN)

하악골 상행지 수직골 절단술 후 마이크로 CT를 이용한 시기별 치유 양상 연구

<지도교수 정 영 수>

연세대학교 대학원 치의학과

오 민 석

상행지 수직골 절단술(Vertical ramus osteotomy, VRO)는 하악골 전돌증 환자에 있어서 임상적으로 많이 사용되는 술식이다. 통상의 외상성 골절편 치유과정과는 근본적으로 여건이 다른 VRO 후 비고정 상태에서 조기 운동 시의 골편 치유과정과 예후에 대하여 임상적 경험에 의존해 왔다고 해도 과언이 아니며, 임상적 여건과 유사한 상태에서의 골치유 및 골개조 양상에 관한 실험적 연구가 부족한 상태이다. VRO의 보다 많은 적용과 올바른 치료를 위해서 이를 실험적으로 규명하는 작업이 꼭 필요하다 판단된다.

이에 최근에 이용빈도가 높아지고 있는 micro computed-tomography (micro-CT)를 이용하여 VRO 후 beagle dog에서 골치유 및 골개조의 시기별 변화 과정을 관찰하고 연구하였다.

VRO를 시행한 7마리의 성견 비글독을 각각 1주, 2주, 3주, 4주, 6주, 8주에 안락사 시킨 뒤 표본을 적출하였다. 각각의 절편은 micro-CT scanner로 촬영하여

영상을 얻은 후 재건하였다. 이후 원심 골편과 근심 골편에서 생긴 신생골로 분류하여 계측하고 여러가지 parameter 들을 산출하였고, 아래와 같은 결론을 얻었다.

1. 전체 신생골은 4 주까지 증가하고 6 주까지 서서히 감소하다가 8 주에는 급격히 감소한다. 이는 통계적으로 유의한 결과를 나타냈다. (Spearman's rank correlation coefficient ; $p < 0.05$)
2. 6 주까지는 원심 골편 주위에서 활발히 신생골이 생겨나지만 8 주에는 그 양상이 역전된다.
3. Micro-CT 를 이용하여 산출한 Parameter 들은 6 주까지 원심 골편 주위에서 생성된 신생골에 대해서 BV (bone volume), BV/TV (bone volume fraction), BS/BV (specific bone surface), Tb.N (trabecular number), Tb.Sp (trabecular separation) 이 통계적으로 의미있는 결과를 나타냈고, 근심 골편 주위에서는 Tb.Th (trabecular thickness)가 통계적으로 의미있는 결과를 나타냈는데, 이는 신생골이 성숙해지면서 강도가 더 강해지는 것을 의미한다.

이상의 결과를 종합해 볼 때 상행지 수직골 절단술의 골치유는 상행지 수직골 절단술의 골치유는 술후 4 주까지는 활발히 신생골이 생기고 이후 재형성 과정을 시작하고, 술후 6 주가 지나면서 가속되는 골치유 양상을

나타내고, 술후 6 주까지는 원심 골편 주위에서 생긴 신생골의 양이 더 많으나, 8 주에는 그 양상이 역전된다.

임상적으로 VRO 시술 시 초기 치유에서 중요한 부분을 담당하는 원심 골편의 혈류를 보존하는데 더 주의를 기울여야 할 것으로 사료된다.

핵심되는 말: 상행지 수직골 절단술, micro-CT, 골치유